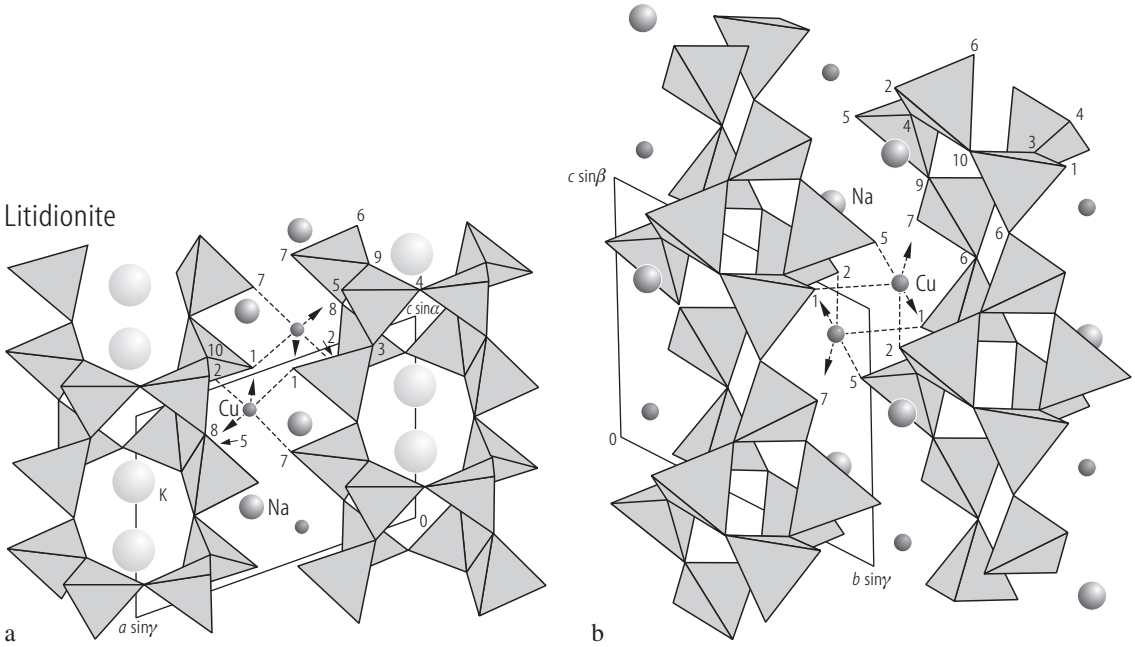

Fig. 1. Litidionite. Crystal structure projected along [010] **(a)** and [100] (**b)**. In **(a)** the bonds terminated by an arrow refer to oxygen atoms O1 and O5 occurring in chains which are not shown. In **(b)** the bonds terminated by an arrow refer to oxygen atoms O1 and O7 occurring in chains which also are not shown. The K atoms have been omitted for clarity [75P1].

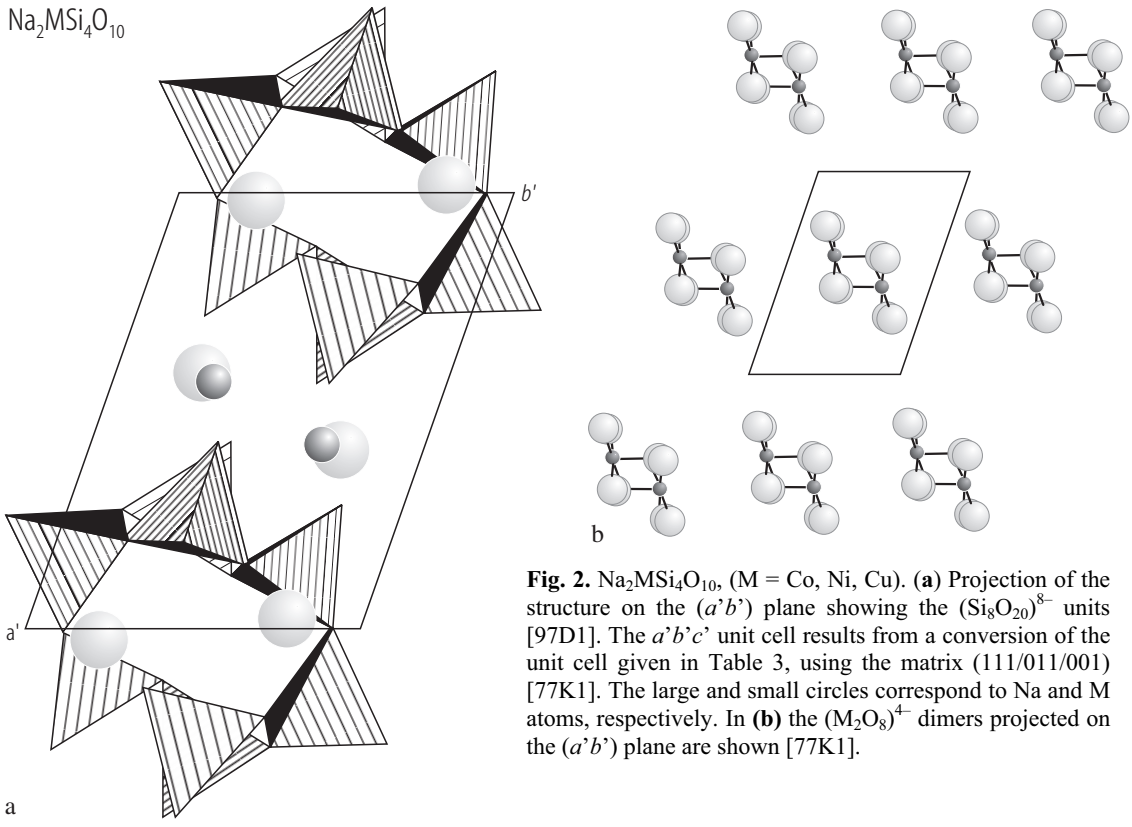

Fig. 2. $Na_2MSi_4O_{10}$, (M = Co, Ni, Cu). (**a**) Projection of the structure on the (*a*'*b*') plane showing the $(Si_8O_{20})^{8-}$ units [97D1]. The *a*'*b*'*c*' unit cell results from a conversion of the unit cell given in Table 3, using the matrix (111/011/001) [77K1]. The large and small circles correspond to Na and M atoms, respectively. In **(b)** the $(M_2O_8)^{4-}$ dimers projected on the (*a*'*b*') plane are shown [77K1].

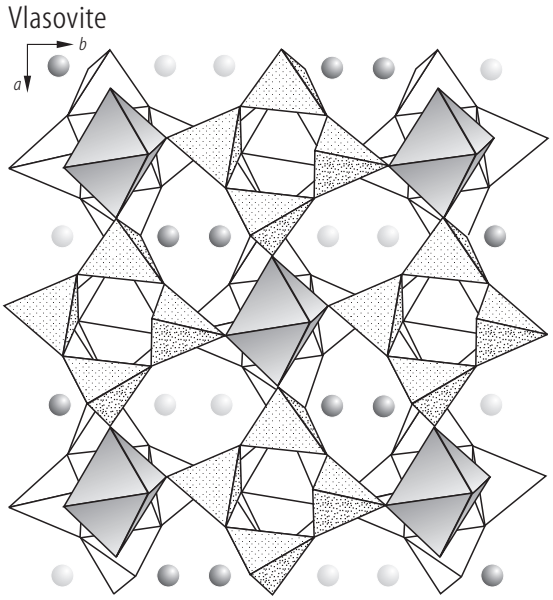

Fig. 3. Vlasovite. Projection of the structure along the [001] axis. Two stories of the heterogeneous Si, Zr framework and also two types of Na atoms in the channel are distinguished here [74V1].

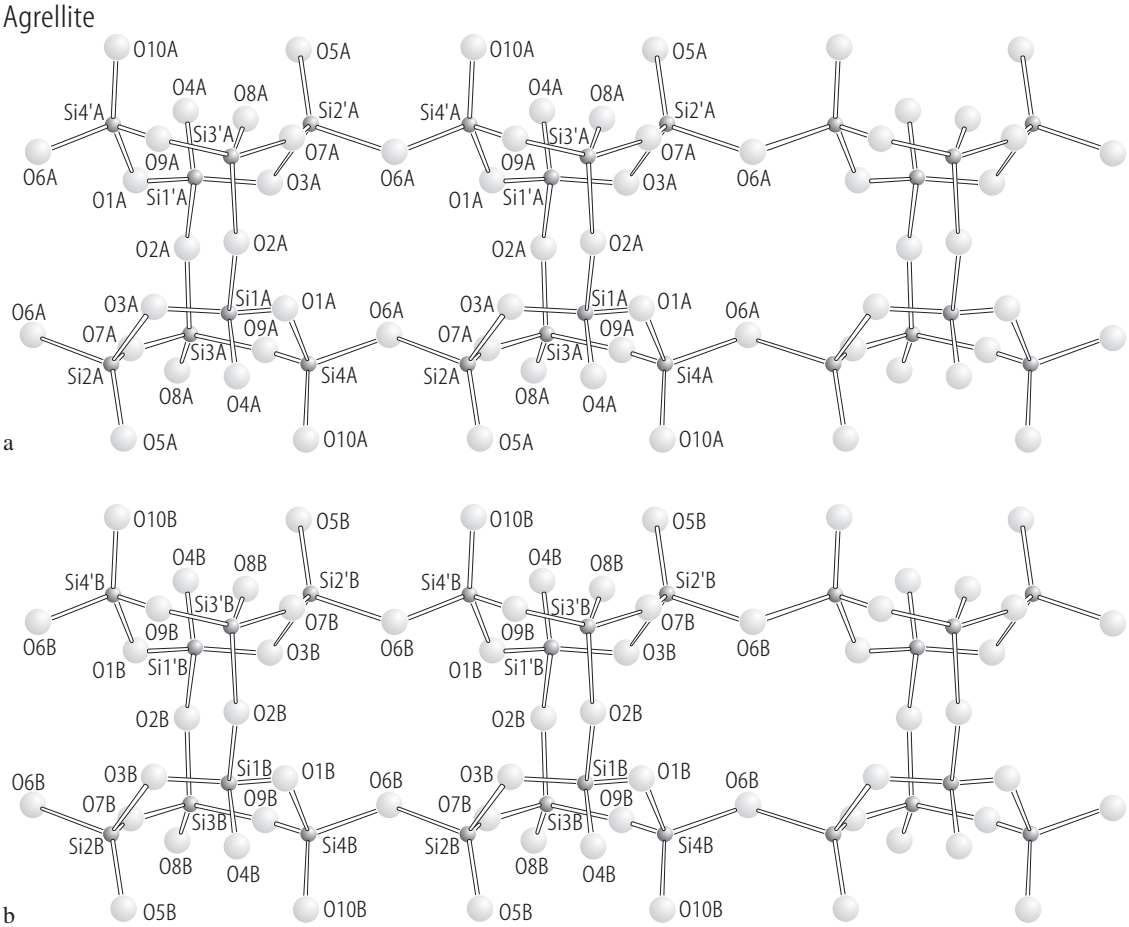

Fig. 4. Agrellite. Stereochemical configuration of two crystallographically different $[Si_8O_{20}]$ double chains (tubes) A and B [79G1].

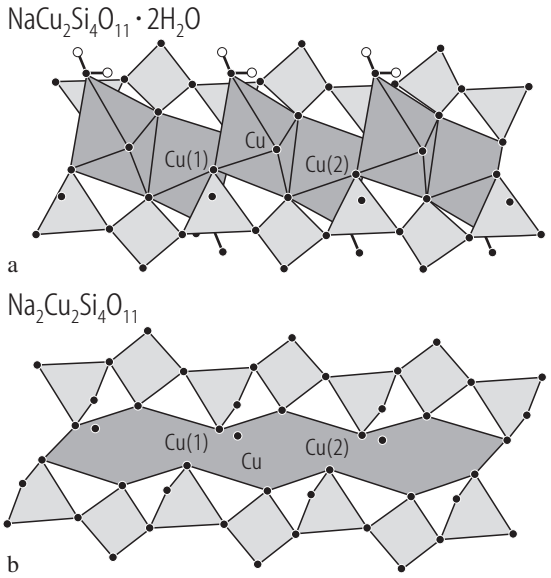

Fig. 5. $Na_2Cu_2Si_4O_{11}·2H_2O$ (**a**) and $Na_2Cu_2Si_4O_{11}$ (**b**). Fragments of the crystal structures comprised of CuO_6 octahedra, SiO_4 tetrahedra and H_2O molecules in ball- and stick representation [05M1].

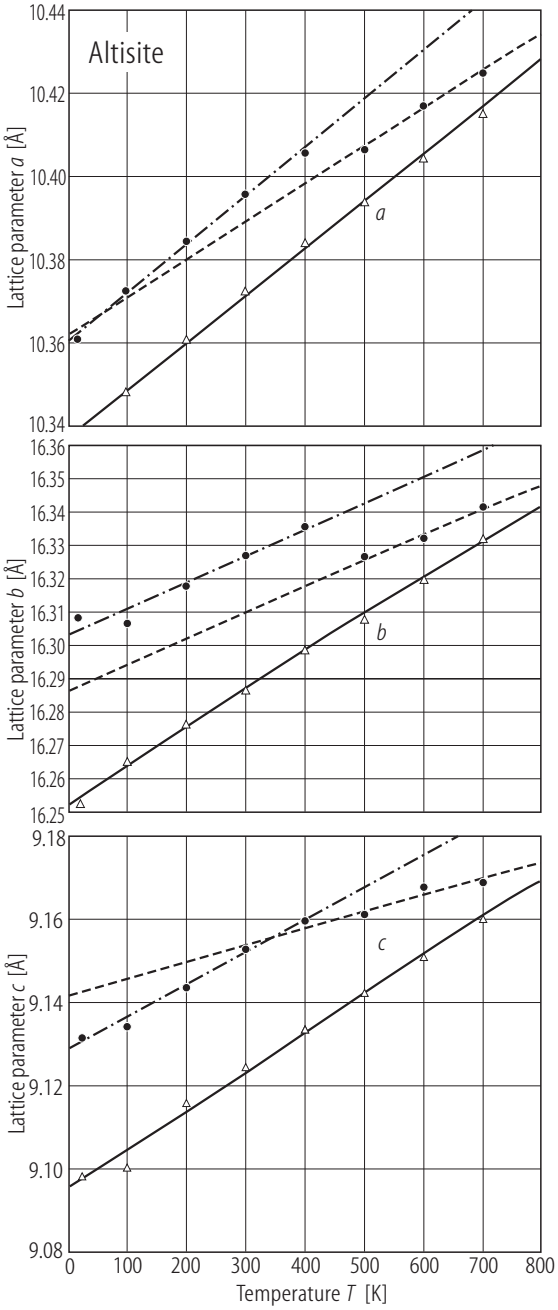

Fig. 6. Altisite. Temperature dependences of the lattice parameters during heating (dots) and cooling (triangles). At 700°C, dots and triangles represent the values before and after equilibration, respectively [95F1]. Two regression lines are shown for increasing temperature in the ranges 20…400°C (dot-dashed) and 500…700°C (dashed).

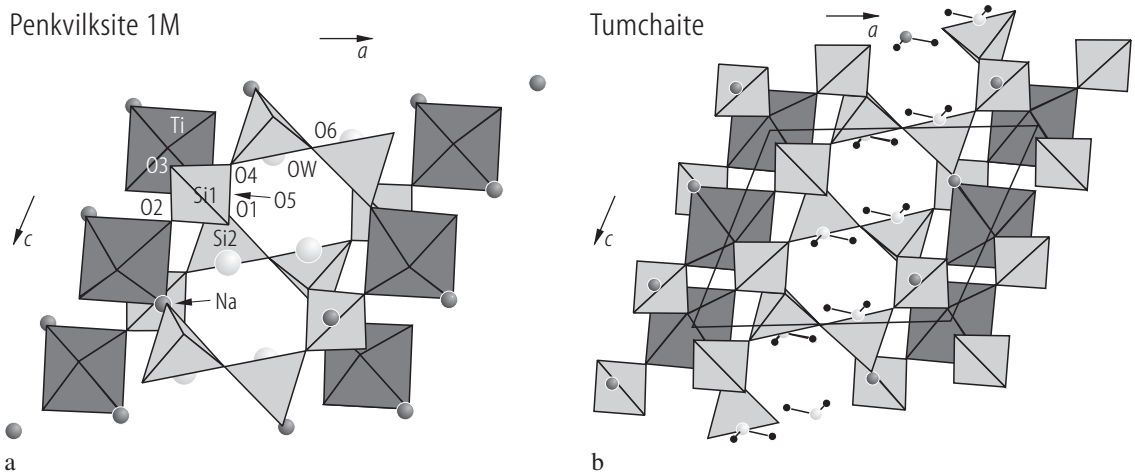

Fig. 7. Penkvilksite 1M **(a)** [94M1], tumchaite **(b)** [00S1]. Crystal structures as seen along [010]. In **(a)** the SiO_4 tetrahedra and TiO_6 octahedra are featured. In **(b)** dark gray circles correspond to Na cations, ZrO_6 octahedra are dark gray, SiO_4 tetrahedra are shown as light gray, water molecules are shown as open circles (O-anions) connected by solid lines with small black circles (H-cations).

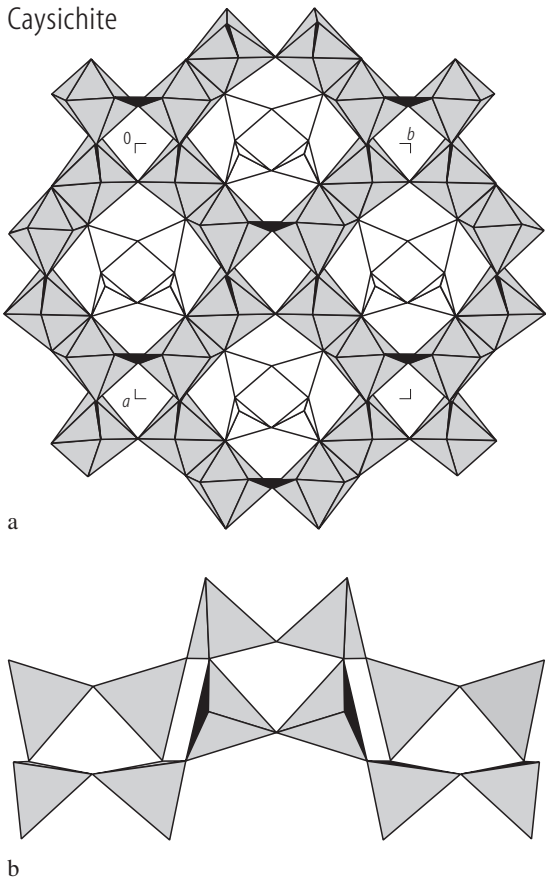

Fig. 8. Caysichite. **(a)** Crystal structure projected on (001). Shading indicates Y and CaR polyhedra, while Si tetrahedra are not shaded, black triangles are C2 carbonate groups and heavy lines indicate C1 carbonate groups; **(b)** the four-repeat double chain of silicon tetrahedra projected on (110) [78M1].

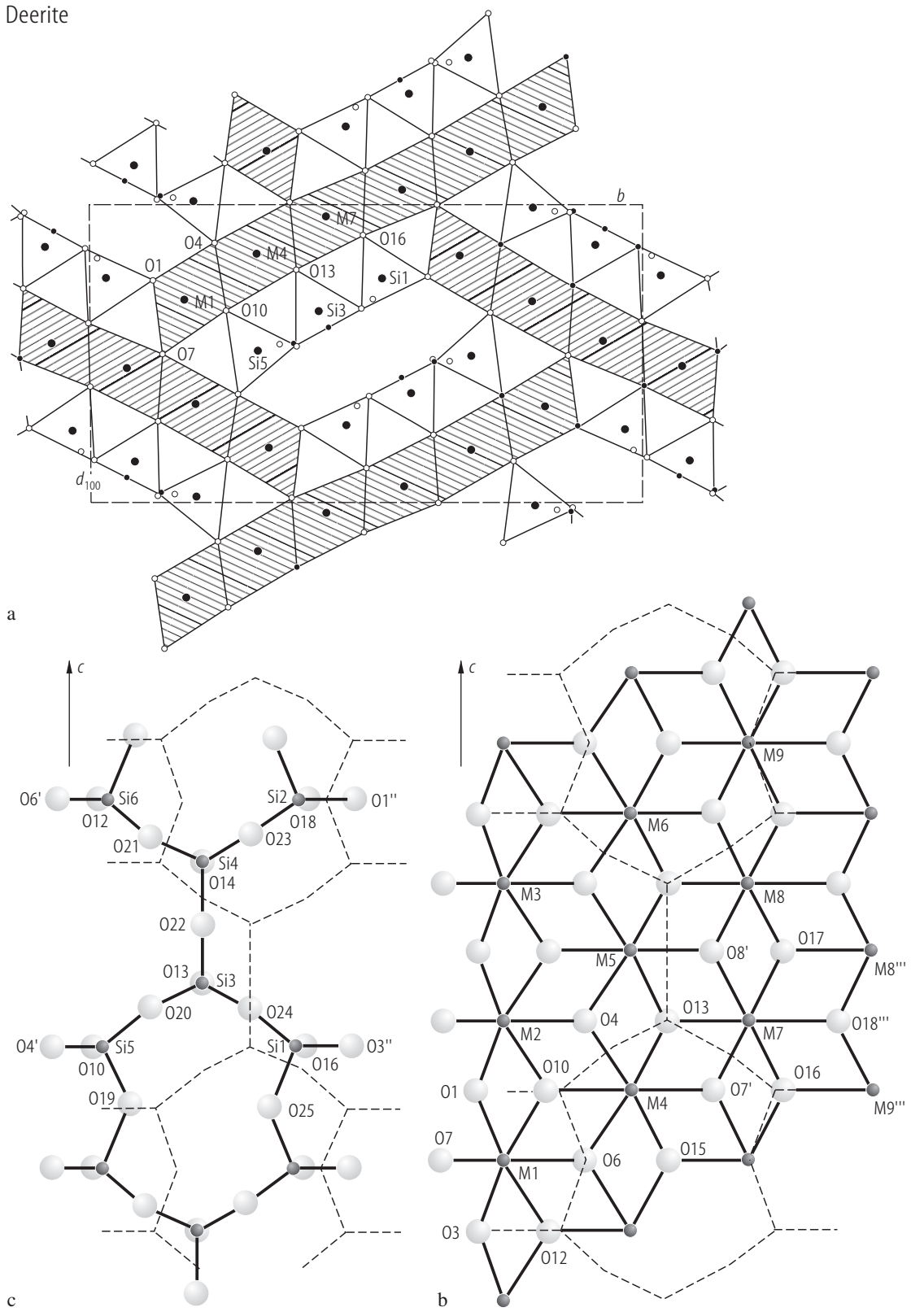

Fig. 9a,b,c. For caption see next page.

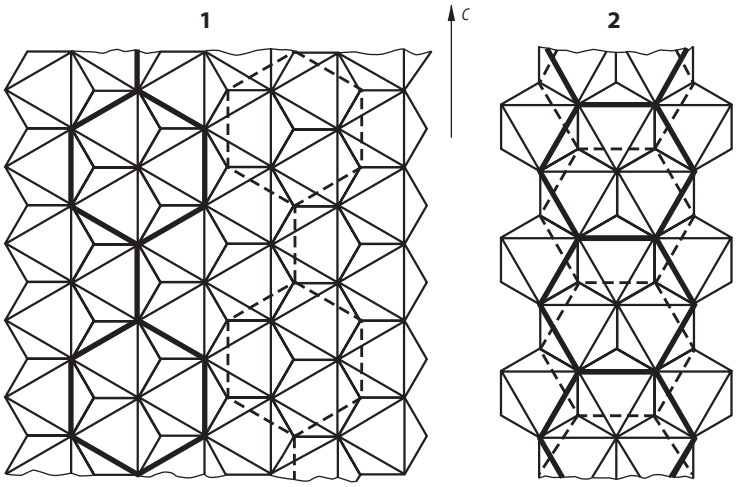

d

Fig. 9. Deerite. **(a)** ***c***-axis projection of the structure. Each M atom and octahedral oxygen represents three superimposed atoms and each Si atom represents two atoms: labels are for lowest of superimposed atoms; bridging tetrahedral oxygens are unlabelled. **(b)** Part of MO_6 octahedral strip projected parallel to (110): broken lines indicate position of $[Si_6O_{17}]$ chain above plane of projection. **(c)** Part of the $[Si_6O_{17}]$ chain projected parallel to (110), positioned relative to the octahedral strip in **(b)**. Broken lines indicate position of the $[Si_6O_{17}]$ chain above the plane of projection (the two silicate chains are back-to-back). **(d)** Relative orientation of the silicate chain and MO_6 octahedra in (1) deerite and (2) amphibole: broken lines indicate silicate-chain position on reverse side of octahedral strip [77F1].

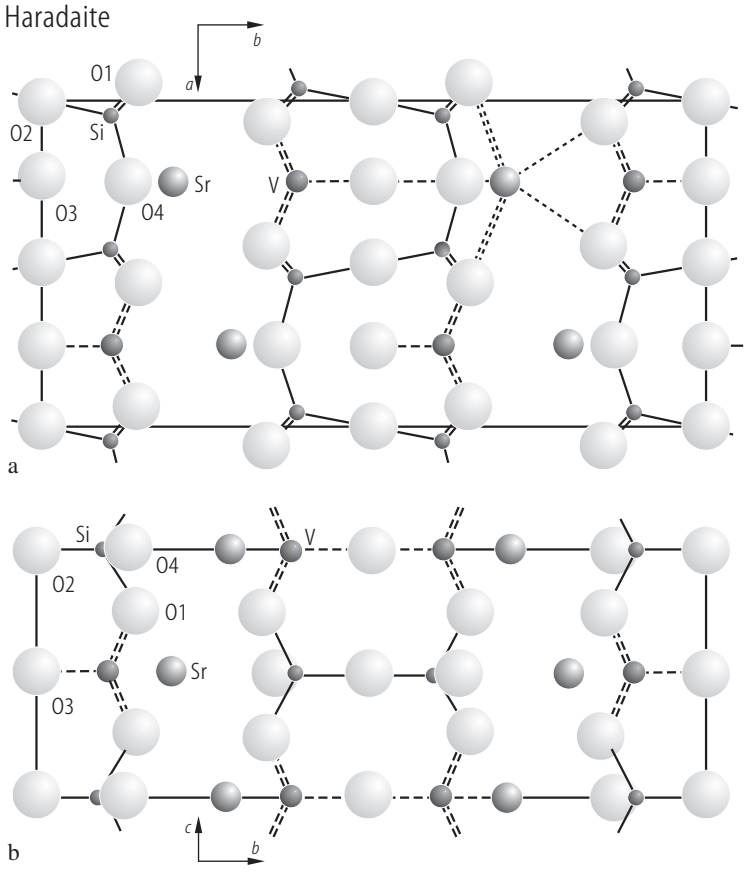

Fig. 10. Haradaite. **(a)** Structure projected along the ***c***-axis and **(b)** along the ***a***-axis. The origin is shifted to (001/2) [67T1].

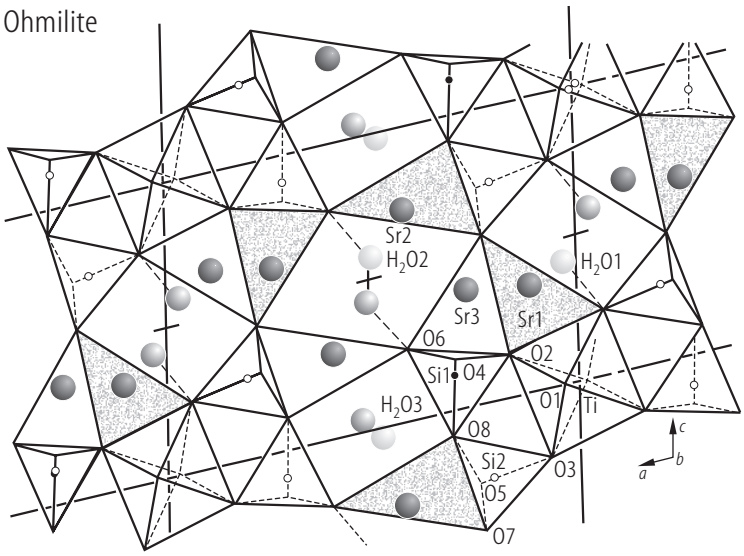

Fig. 11. Ohmilite. Projection parallel to ***b***-axis. Sr atoms (dark gray circles) in stippled triangles are in mirror planes at y = ¼ and those in blank triangles are at y = ¾. Light gray circles and medium gray ones depict oxygens of water molecules and lie in mirror planes at y = ¾ and ¼, respectively. Doubly-dashed lines indicate the two directions of hydrogen bonds corresponding to a water molecule [83M1].

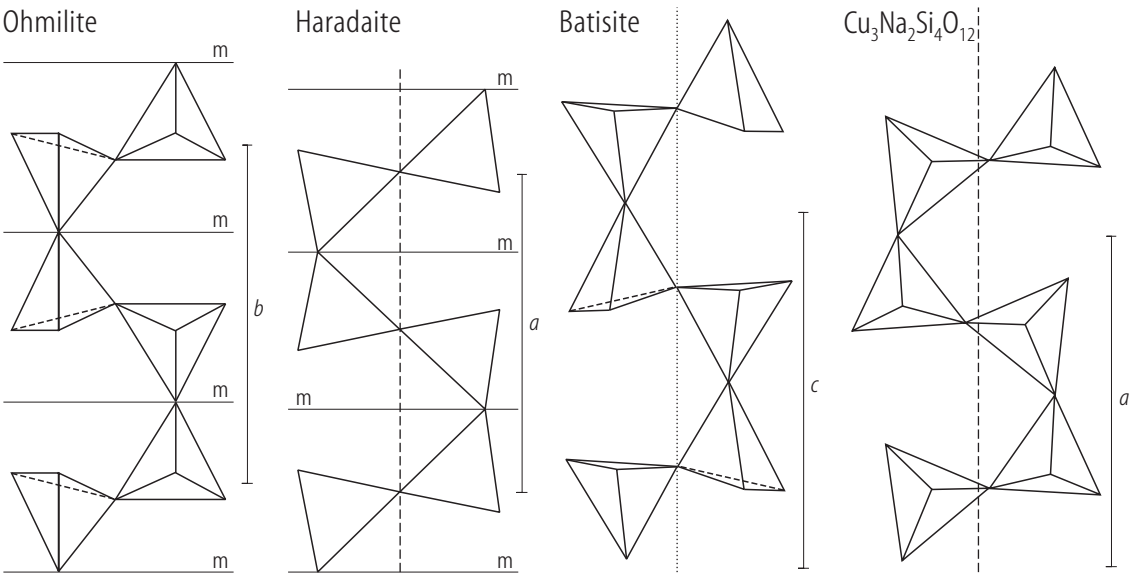

Fig. 12. Si_4O_{12} chains found in ohmilite [83M1], haradaite [67T1, batisite [62N1] and $Cu_3Na_2(Si_4O_{12})$ [76K1]. Broken lines and a dotted line indicate ***a***-glide planes and ***c***-glide planes, respectively. Solid lines with the letter "m" are mirror planes. Unit cell edges along the chain length are shown [83M1].

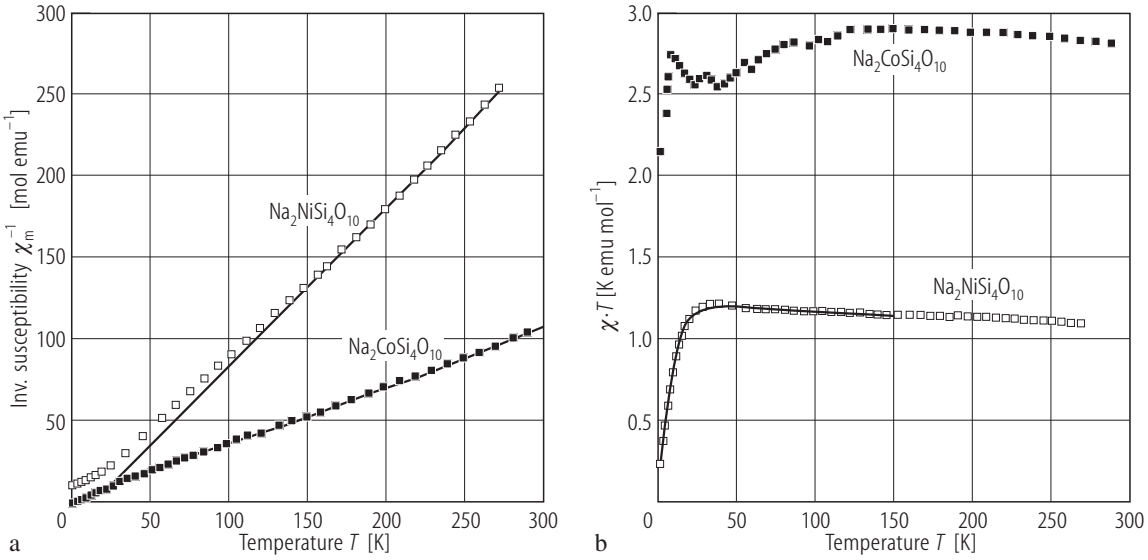

Fig. 13. $Na_2MSi_4O_{10}$, (M = Co, Ni). **(a)** Temperature dependences of the inverse magnetic susceptibilities. **(b)** χT product evolutions. The continuous line for the Ni sample represents the fitted $\chi T = f(T)$ curve [97D1].

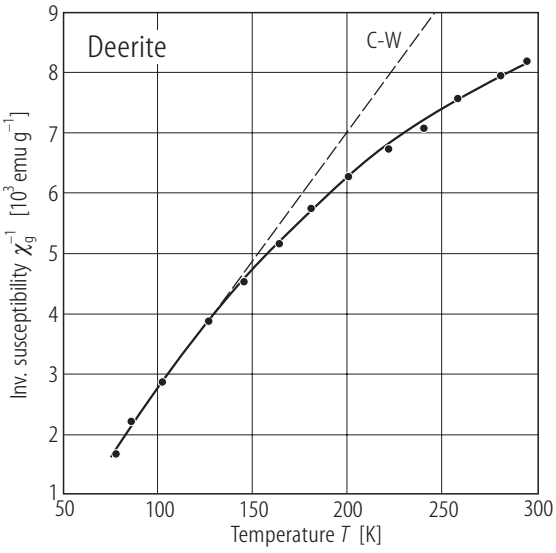

Fig. 14. Deerite. Temperature dependence of the inverse susceptibility [66C1].

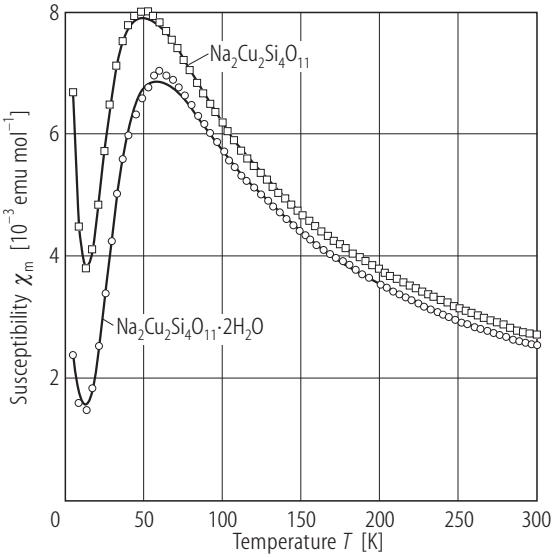

Fig. 15. $Na_2Cu_2Si_4O_{11}\cdot 2H_2O$ (open circles) and $Na_2Cu_2Si_4O_{11}$ (squares). Thermal variations of magnetic susceptibilities determined in a field $\mu_0 H$ = 1 T. Full lines are fits as described in text [05M1].

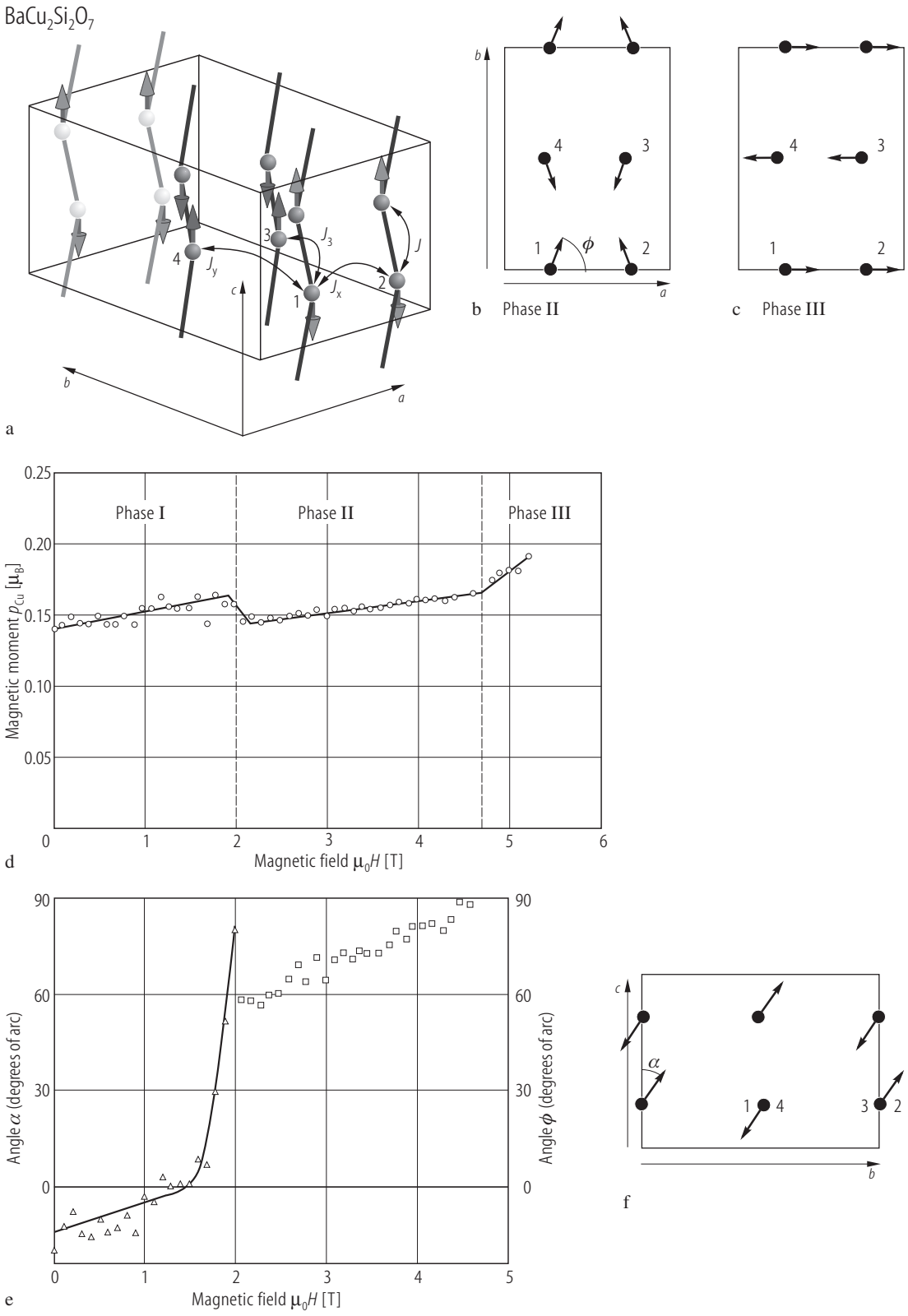

Fig. 16. For caption see next page

Fig. 16. $BaCu_2Si_2O_7$. Schematic views of the magnetic structure in: (**a**) zero-field and (**b**,**c**) in magnetic fields applied along the ***c***-axis. In (**a**) the $S = 1/2$ Cu^{2+} ions form slightly zig-zag antiferromagnetic chains. In (**b**,**c**) the spin structures in phase II for $H_{c1} < H < H_{c2}$ with $\mu_0 H_{c1} = 2$ T and $\mu_0 H_{c2} = 4.7$ T and phase III for $H > H_{c2}$ are given. The spins are largely confined to the (a,b) crystallographic plane [02Z1]. In (**d**) is given the field dependence of the ordered moment and in (**e**) the tilt angle α in phase I and casting angle ϕ in phase II. The tilting of spin structure in the field $H < H_{c1} = 2$ T applied along the ***c***-axis (phase I) is shown in (**f**). The spins are largely confined to the (b,c) crystallographic plane [02Z1].

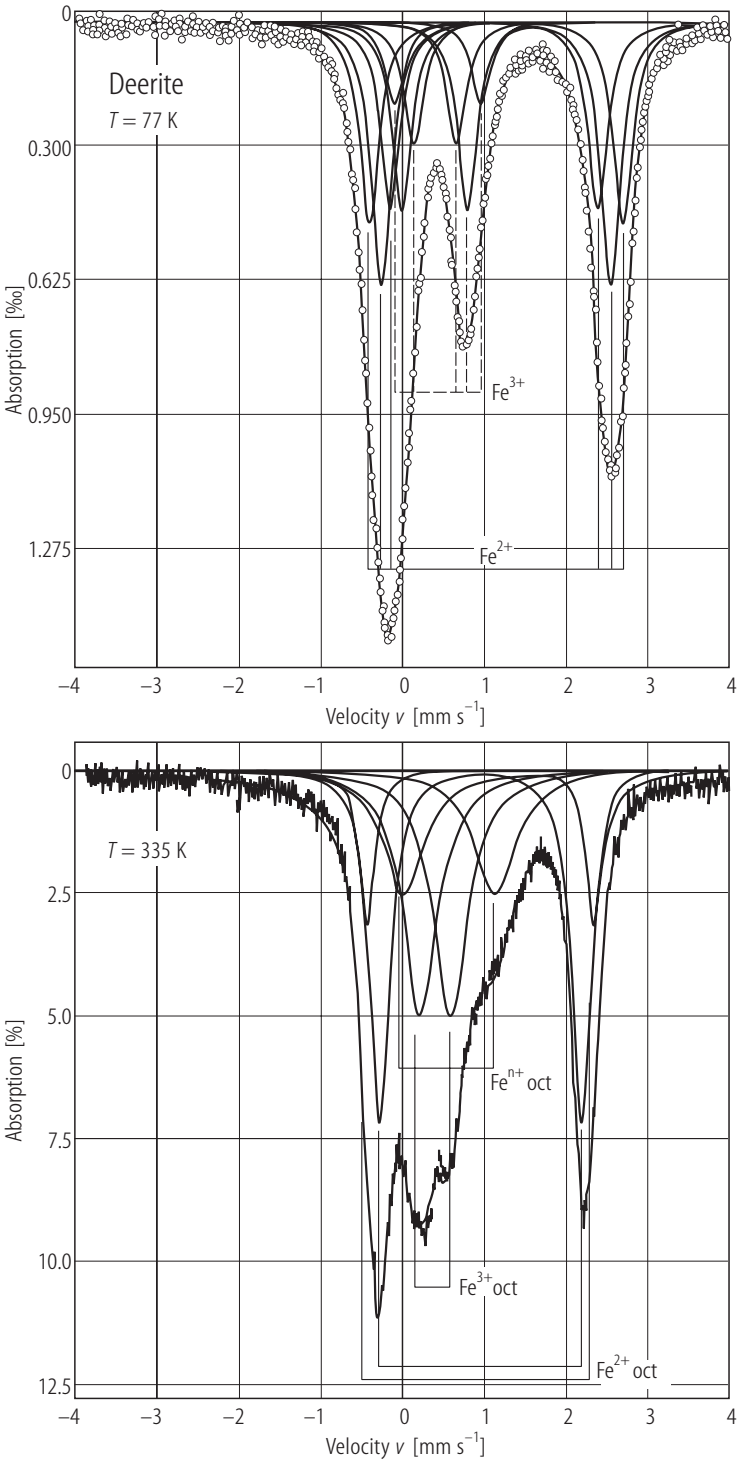

Fig. 17. Deerite[2)]. ^{57}Fe NGR spectra at 77 K **(a)** and 335 K **(b)** [80A1]. Solid lines are least square fits to uncorrected data. - For composition of sample [2)] see footnote of Table 5.

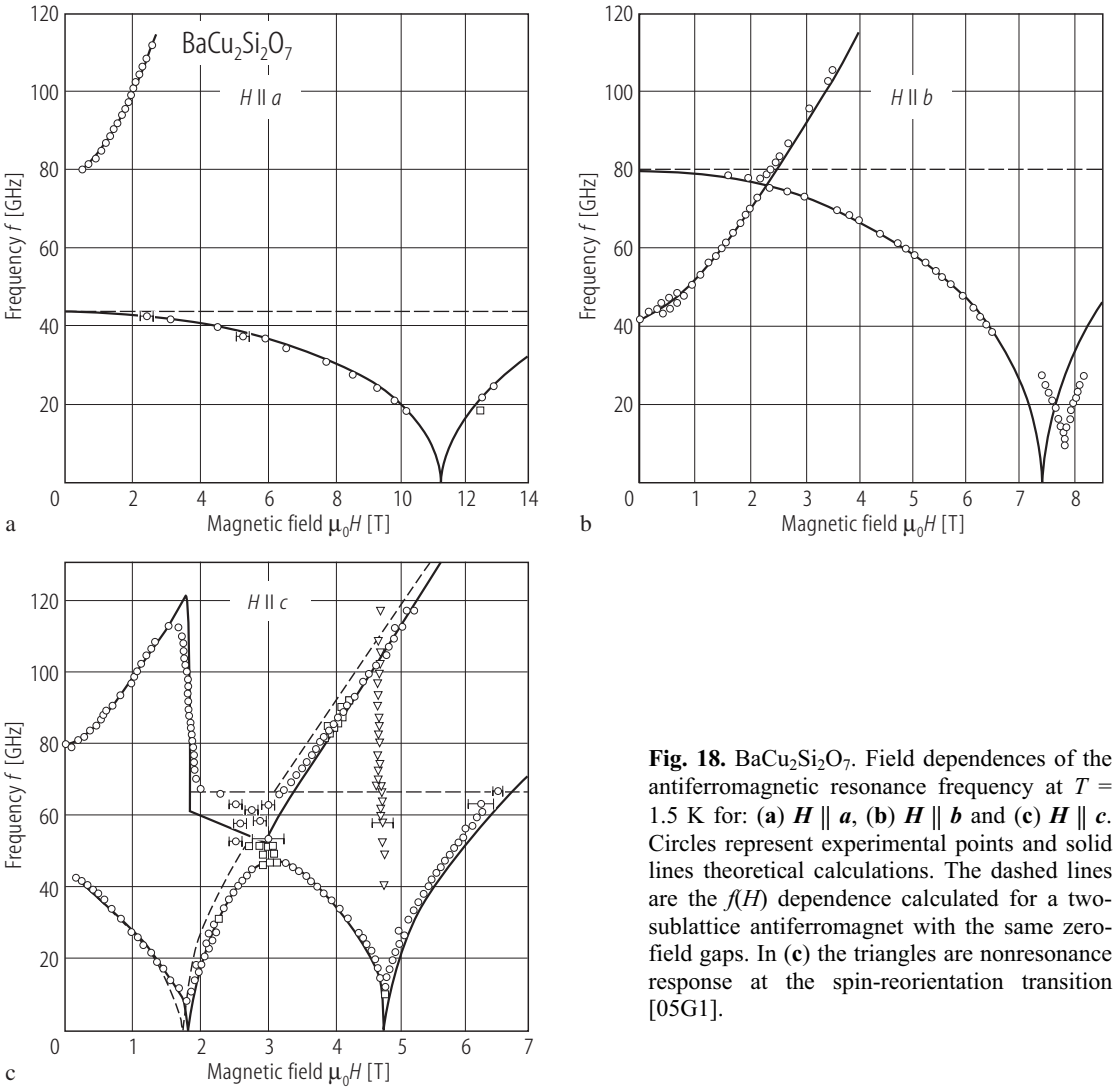

Fig. 18. $BaCu_2Si_2O_7$. Field dependences of the antiferromagnetic resonance frequency at T = 1.5 K for: (**a**) $\boldsymbol{H} \parallel \boldsymbol{a}$, (**b**) $\boldsymbol{H} \parallel \boldsymbol{b}$ and (**c**) $\boldsymbol{H} \parallel \boldsymbol{c}$. Circles represent experimental points and solid lines theoretical calculations. The dashed lines are the $f(H)$ dependence calculated for a two-sublattice antiferromagnet with the same zero-field gaps. In (**c**) the triangles are nonresonance response at the spin-reorientation transition [05G1].

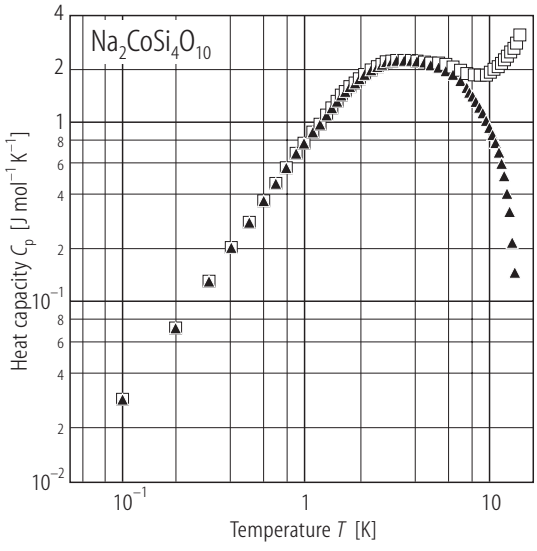

Fig. 19. $Na_2CoSi_4O_{10}$. Heat capacity versus temperature (in a logarithmic representation). The squares represent the experimental points and the triangles the calculated heat capacity of magnetic origin [97D1].

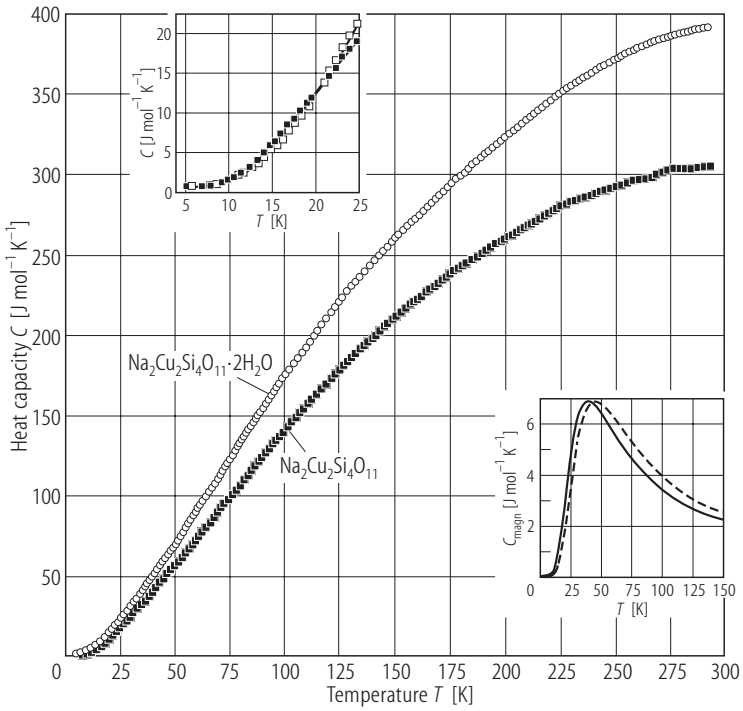

Fig. 20. $Na_2Cu_2Si_4O_{11}·2H_2O$ (open symbols) and $Na_2Cu_2Si_4O_{11}$ (full symbols). Temperature dependences of the heat capacity. The inset at the top zooms on the low-temperature data. The inset at the bottom presents calculations of the magnetic heat capacity for both systems (dashed-hydrated; solid-dehydrated) [05M1].

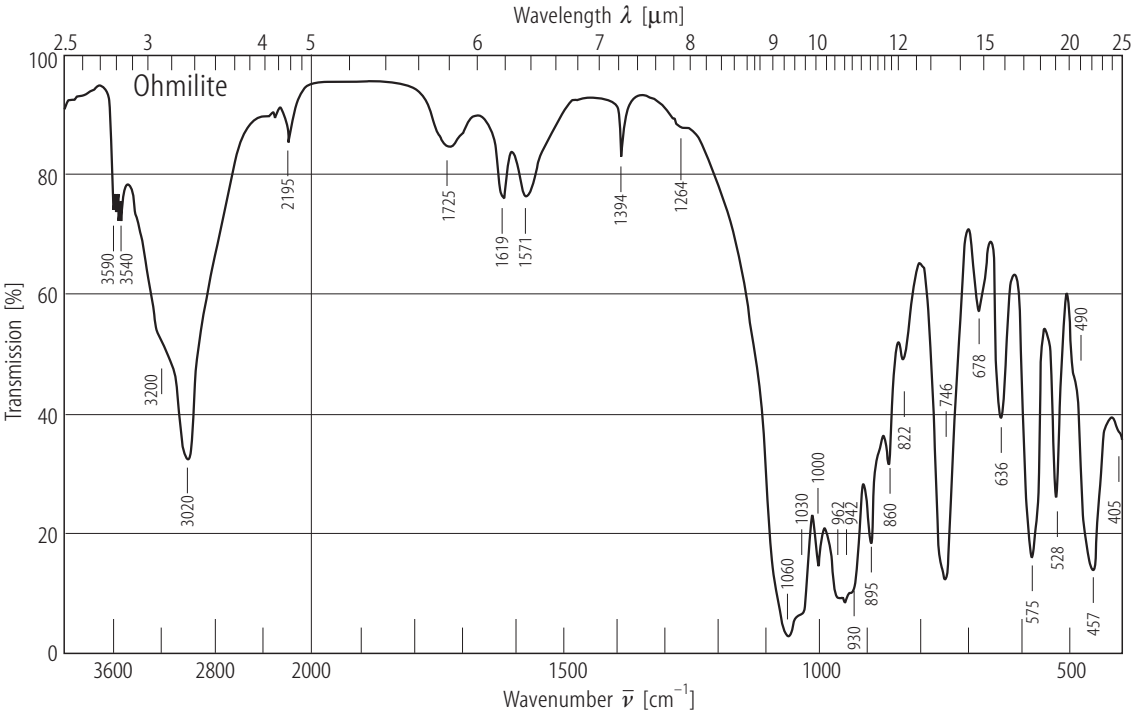

Fig. 21. Ohmilite. Infrared absorption spectrum [83M1].